J. Marine Sci. Appl. (2013) 12: 89-97
DOI: 10.1007/s11804-013-1171-z

Numerical Simulation of Motion Response of an Offshore Observation Platform in Waves

Yuanchuan Liu and Decheng Wan*

State Key Laboratory of Ocean Engineering, School of Naval Architecture, Ocean and Civil Engineering, Shanghai Jiao Tong University, Shanghai 200240, China

Abstract: Offshore observation platforms are required to have great ability to resist waves when they are operating at sea. Investigation on the motion characteristics of the platforms in the sea can provide significant reference values during the platform design procedure. In this paper, a series of numerical simulation on the interaction of a triple-hulled offshore observation platform with different incident waves is carried out. All of the simulations are implemented utilizing our own solver naoe-FOAM-SJTU, which is based and developed on the open source tools of OpenFOAM. Duration curves of motion characteristics and loads acting on the platform are obtained, and a comparison between the results of the amplitude in different incident waves is presented. The results show that the solver is competent in the simulation of motion response of platforms in waves.

Keywords: offshore observation platform; motion characteristics; naoe-FOAM-SJTU solver; finite volume method (FVM); pressure-implicit-split-operator (PISO)

Article ID: 1671-9433(2013)01-0089-09

1 Introduction

The safety and effectiveness of a working offshore observation platform are closely related to its motion characteristics in waves. To a platform spending most of its time operating at sea, excessive motion amplitude not only will influence the safety of the structure, but also leads it to fail to provide embarked instruments and equipment with appropriate working conditions. If the motion characteristics are predicted accurately for adequate time; then improvements and adjustments can be made during the design procedure. Consequently, investigation on the motion characteristics of offshore observation platforms is of great significance.

Along with the development of computer hardware and computing technology, numerical simulation, other than performing model tests in a physical wave tank, has gradually become a common alternative to study the motion characteristics of naval and ocean structures in waves.

Conventional simulation often applies methods based on the potential flow theory. Due to the relatively fast speed and effective estimation, these methods have been widely used in motion prediction. They include strip theory (He *et al.*, 1998), 3-D frequency domain methods (Chen, 2011), time domain methods (Chen and Zhu, 2010) and so forth. But these methods have limits, too. For example, viscosity is overlooked and nonlinear factors usually cannot be taken into account. On the contrary, CFD methods always consider the effects of both viscosity and nonlinearity; hence the results should be accurate. In recent years, CFD methods have been increasingly applied to deal with the motion problems of offshore structures. Wu *et al.* (2008) simulated wave-induced ship motions in regular head waves, and the results achieved good agreement with those of model tests. Shen *et al.* (2011) performed a series of numerical ship model simulations based on open source code and established a benchmark. Yang *et al.* (2011) implemented the simulation of DTMB 5512 ship model's coupled pitch & heave motions in two regular waves of different wave height, and calculated the response amplitude operators.

In this paper, a series of numerical simulation on the interaction of a triple-hulled offshore observation platform with different incident waves is conducted. Duration curves of the platform's coupled motion of pitch & heave, roll motion, forces and moments acting on it are obtained. And a comparison between the results of the amplitude in incident waves of different wave height and length is drawn.

As for numerical methods, the finite volume method (FVM) is applied to discretize the governing equations; free surface is captured by volume of fluid (VOF) method, and the pressure-implicit-split-operator (PISO) algorithm is utilized for pressure-velocity decoupling. To compute the motion of the platform, the six degree of freedom (6DOF) kinematic equations are solved. The dynamic mesh deformation technique is also employed to simulate the movement of the platform. All of the computation is executed using our own solver naoe-FOAM-SJTU, which is based on the open source tools of OpenFOAM and developed by our team. Several modules (Shen *et al.*, 2012) have been integrated into the naoe-FOAM-SJTU solver to accomplish complex

Received date: 2012-06-11.
Foundation item: Supported by the National Natural Science Foundation of China (Grant No. 50739004 and 11072154), Foundation of State Key Laboratory of Ocean Engineering of China (GKZD010059), the Program for Professor of Special Appointment (Eastern Scholar) at Shanghai Institutions of Higher Learning (2008007), and The Lloyd's Register Educational Trust (The LRET).
***Corresponding author Email:** dcwan@sjtu.edu.cn

computations. The wave generation module is used for generating wave satisfying required standards; the 6DOF motion module serves for calculating motions and forces of structures, and the dynamic mesh deformation module can deform mesh cells to simulate movement of structures. This solver has already been applied and validated in previous contributions, such as numerical wave generation and absorption (Cha and Wan, 2011), simulation of 3-D flow past single and two tandem circular cylinders (Cao and Wan, 2010), simulation of solitary wave impact on fixed offshore platform (Cao *et al.*, 2011) and so on. Good accuracy of results is shown in all the research. Therefore, reliability of the solver can be guaranteed and it can be used for simulation with confidence.

2 Numerical methods

2.1 Governing equations

For unsteady, incompressible and viscous fluid flows, the governing equations are as follows:

$$\nabla \cdot \boldsymbol{U} = 0 \tag{1}$$

$$\frac{\partial(\rho \boldsymbol{U})}{\partial t} + \nabla \cdot (\rho(\boldsymbol{U} - \boldsymbol{U}_g)\boldsymbol{U}) = -\nabla p_d - g \cdot \boldsymbol{x} \nabla \rho + \nabla \cdot (\mu \nabla \boldsymbol{U}) + \boldsymbol{f}_\sigma + \boldsymbol{f}_s \tag{2}$$

where $\boldsymbol{U}$ and $\boldsymbol{U}_g$ stand for velocity field and mesh moving velocity respectively; $p_d = p - \rho g \cdot \boldsymbol{x}$ represents dynamic pressure; ρ, g and μ denote density of fluid, gravity acceleration vector and dynamic viscosity separately; $\boldsymbol{f}_\sigma$ is the free surface tension term which will be specified in section 2.2; and $\boldsymbol{f}_s$ is the source term for wave damping in a wave damping zone of numerical wave tank.

2.2 VOF method

In this work, VOF method (Rusche, 2002) is applied to capture the free surface. This method has the advantage of being able to control numerical diffusion and can also provide high accuracy. The transport equation for α is defined as follows:

$$\frac{\partial \alpha}{\partial t} + \nabla \cdot \left[\left(\boldsymbol{U} - \boldsymbol{U}_g \right) \alpha \right] + \nabla \cdot \left[\boldsymbol{U}_r (1 - \alpha) \alpha \right] = 0 \tag{3}$$

where the first two terms represent the volume fraction term in continuous equation, and the last term stands for the compressible term when free surface is considered. α denotes the volume fraction which is the volume percentage of liquid in one cell. To all of the cells, the value of α varies between 0 and 1:

$$\begin{cases} \alpha = 0 & \text{air} \\ \alpha = 1 & \text{water} \\ 0 < \alpha < 1 & \text{interface} \end{cases} \tag{4}$$

With the introduction of α, ρ and μ can be defined as:

$$\rho = \alpha \rho_l + (1 - \alpha) \rho_g \tag{5}$$

$$\mu = \alpha \mu_l + (1 - \alpha) \mu_g \tag{6}$$

where the subscripts of g and l represent gas and liquid separately.

The free surface term in Eq. (2) can be written as:

$$\boldsymbol{f}_\sigma = \sigma \kappa \nabla \alpha \tag{7}$$

where σ is the free surface tension whose value is σ=0.07 kg/s^2, and the curvature of free surface is denoted by $\kappa = -\nabla \cdot (\nabla \alpha / |\nabla \alpha|)$.

2.3 Discretization

In this work, both governing equations and VOF transport equation are discretized by the FVM. The computation domain is divided into separate cells. The flow field data are stored in the center of the cell; interpolation calculation is then operated to get the data in the faces of the cell, and area integral is performed to obtain the data in the whole domain. The discretization schemes applied in Eq. (2) are second-order upwind scheme for the convection term and second-order central scheme for the diffusion term; Van Leer scheme is used in Eq. (3) and the time derivative terms in both equations are discretized by Euler scheme.

2.4 Velocity-pressure decoupling

The PISO algorithm (Issa, 1986) is utilized for velocity-pressure decoupling (VPD). The algorithm is originally used for unsteady and compressible flow, but later imported to solve steady and incompressible fluid problems. The whole process is divided into three steps: predict – correct – re-correct.

2.5 6DOF motion

A 6DOF motion solver (Shen and Wan, 2011, 2012) is employed to compute the motion of the platform. During the process, two coordinate systems (Carrica *et al.*, 2007) are used: the earth fixed coordinate system and the platform fixed coordinate system. The origin of the earth fixed coordinate system is located in the bow end of the waterline when the platform is under upright floating condition. The positive direction of the *X*-axis points to the stern; positive *Z*-axis is vertically upward, and the direction of *Y*-axis complies with the right-hand rule. The two coordinate systems coincide with each other under upright floating condition. Details about this process can be found in the listed references (Wilson *et al.*, 2006; Carrica *et al.*, 2011).

2.6 Dynamic mesh deformation technique

The dynamic mesh deformation technique is designed to simulate the movement of the platform. During computation, the topological relationship among cells remains unchanged, while cells will translate, stretch and deform. Positions of all cells in the flow field are obtained by solving the following Laplace equation:

$$\nabla \cdot (\gamma \nabla \boldsymbol{U}_g) = 0 \tag{8}$$

where γ is the function of r, which is the distance from the

center of a cell to the surface of the platform:

$$\gamma = \frac{1}{r^2} \tag{9}$$

3 Model and working conditions

3.1 Computation model

The computation model used in this study is a triple-hulled offshore observation platform as shown in Fig. 1. The platform consists of one large cylinder structure and two other small ones, together with deck and panels connecting the deck and cylinders. In calm water, free surface passes through the center lines of these cylinders. Main parameters of the platform are listed in Table 1.

Table 1 Main parameters of platform

Parameter	Value
Length/m	14
Width/m	10
Air gap/m	2
Diameter of large cylinder/m	2
Diameter of small cylinders/m	1.4
Displacement/m^3	28.975

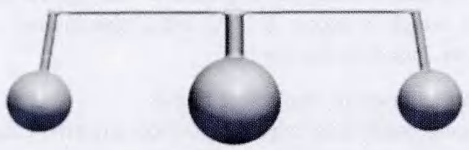

(a) Front view

(b) Left view

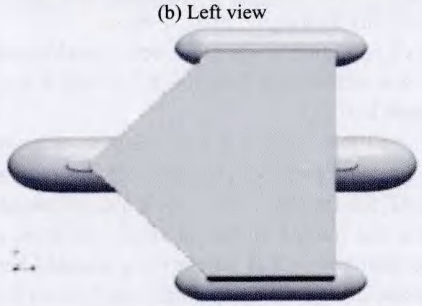

(c) Top view

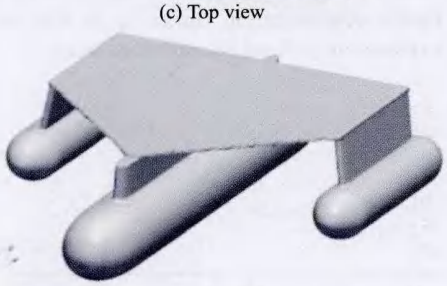

(d) 3-D view

Fig. 1 Computation model

3.2 Working conditions

Four working conditions are considered in this work, and two types of motions are simulated under each condition, i.e., coupled motion of pitch & heave as well as roll motion. Wave parameters of each condition are listed in Table 2.

Table 2 Wave parameters

No. of working condition	Wave length λ/m	Wave height H/m	Period T/s
1	14	0.5	3
2	14	1	3
3	35	1	4.7
4	35	2	4.7

4 Computation mesh

Computation mesh is generated using a utility called snappyHexMesh, which is provided by OpenFOAM and used to generate block-structured mesh. The basic procedure is as follows: platform is first modeled by a 3-D modeling software; background mesh is then generated under Cartesian coordinate system; and finally, the platform is tessellated into the background mesh by the utility. Most of the cells generated are hexahedron.

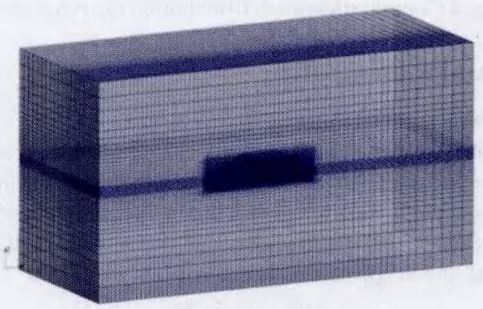

(a) Global mesh

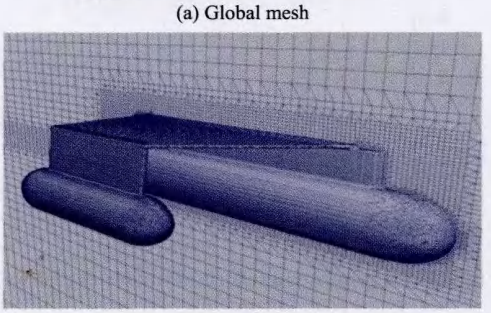

(b) Local mesh

Fig. 2 Computation mesh distribution for coupled motion of pitch & heave

For cases of coupled motion of pitch & heave, with the symmetry characteristics of both geometry and motion patterns in transverse direction taken into account, only half of the platform and computation domains are considered, so as to reduce computation cost. Mesh distribution is presented in Fig. 2. Wave is generated in the left side of the

wave tank and propagates in positive X-axis direction. More cells are distributed both near the free surface and around the platform to improve the accuracy and reliability of the results. Overall number of the grids amounts to a bit more than 300 000.

For the cases of roll motion, since the platform is asymmetric in longitudinal direction, mesh has to be generated for the whole platform. As a result, overall number of the grids is almost doubled than that of cases of pitch & heave. As wave propagates in positive Y-axis direction, it is generated from a different side of the wave tank. Mesh distribution is presented in Fig. 3.

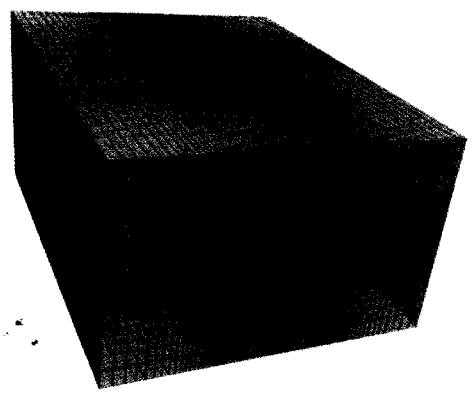

Fig. 3 Computation mesh distribution for roll motion

5 Simulation results

5.1 Wave generation test

Before the simulation of the interaction of platform with incident wave is performed, wave generation tests should be implemented to verify whether the incident wave meets the requirements. Test result under condition 4, i.e., wave length of 35 m and height of 2 m, is presented in Fig. 4.

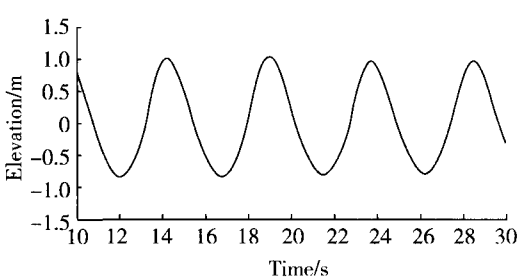

Fig. 4 Wave generation test result under condition 4

Fig. 4 shows that wave crest is about 1 m high and remains nearly undiminished, while wave trough is a little less than 1 m. In consideration of nonlinearity of wave, a conclusion can be made that requirements are basically satisfied.

5.2 Convergence test

To stress the convergence issue, three cases with the same configuration but different grid numbers are simulated as an example. The time step is set to 0.002 s in all three cases. The cases are different in mesh arrangement. Take cell number in 0.2 m near free surface for example, the value is set to 6, 7 and 8 separately, resulting in the total grid number of about 190 000, 318 000 and 433 000 respectively. Results of pitch motion under working condition 4 are shown in Fig. 5.

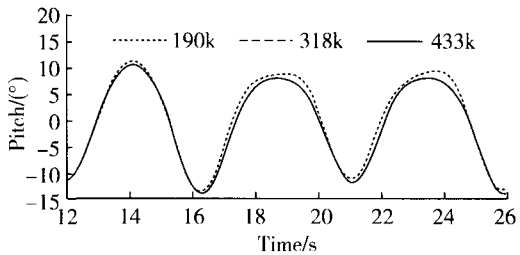

Fig. 5 Convergence test result under condition 4

In Fig. 5, curves representing 318 k and 433 k almost coincide, showing good convergence of results when grid number reaches above 300 000. Results of other variables under different conditions also have similar trend, but are not presented here concerning the limited space. It can be concluded that results are independent of mesh if it's set to about 318 000. It's worth mentioning that CPU time consumed in the case of 318 000 is about 42 000 seconds or nearly 12 hours when the application runs on 16 cores in parallel, which is acceptable. All other simulations will be conducted based on this mesh.

5.3 Coupled motion of pitch & heave

Working conditions can be classified into two categories according to the parameters of incident wave: with same wave length but different wave height, and with same wave height but different wave length. Comparisons will be made for both categories on pitch & heave motion, force in Z-axis direction and moment on Y-axis.

5.3.1 Conditions with different wave height

Results of condition 1 and condition 2, under which wave length is 14 m while wave height is 0.5 m and 1 m separately, are presented in Fig. 6.

Since it will take some time for wave to propagate along the tank, the platform doesn't move fiercely until wave has got there. All the figures in this article are processed to begin from where the motion of the platform becomes relatively stable, and data before that time is not presented here, which will not make a big difference to the analysis of the results. When similar representation comes up in the rest of this article, explanation will not be made explicitly.

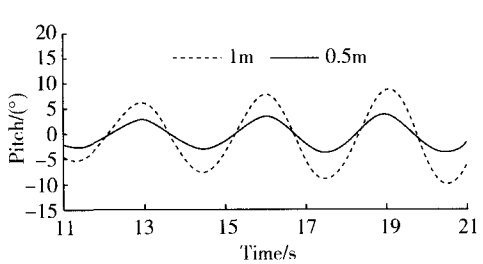

(a) Duration curve of pitch motion

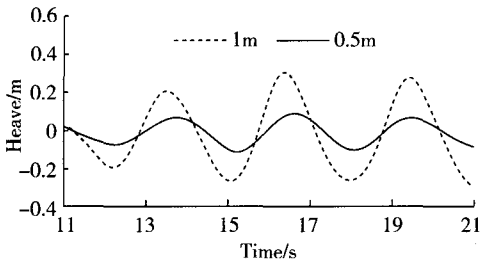

(b) Duration curve of heave motion

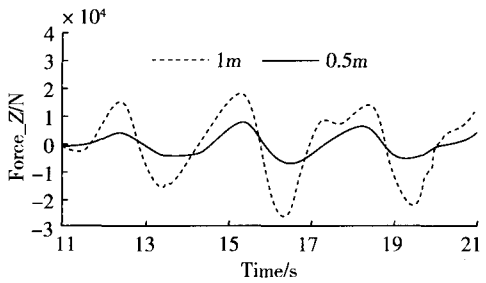

(c) Duration curve of force in *Z*-axis direction

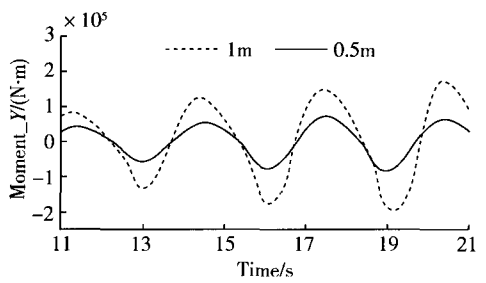

(d) Duration curve of moment on *Y*-axis

Fig. 6 Coupled motion of pitch & heave and loads duration curves under conditions with different wave heights

In Fig. 6, solid line stands for condition 1 with wave height of 0.5 m, while dashed line for condition 2 with wave height of 1 m. It can be seen from the figures that amplitudes of pitch and heave are about 3.5° and 0.08 m respectively under condition 1. When wave height increases to 1 m, amplitudes become larger and reach 7.9° and 0.3 m separately, indicating that amplitude of pitch doubles while that of heave increases much more. A conclusion can be made that heave motion, compared to pitch, is more sensible to the change of wave height. Force and moment vary in similar manners.

In addition, there exists nuance of phase between curves of pitch and heave motion. In other words, when platform reaches the peak of heave motion, it hasn't pitched to the maximum angle. Moreover, difference of phase also can be seen between motions and loads.

5.3.2 Conditions with different wave length

Condition 2 and condition 3 have same wave height of 15 m but different wave length of 14 m and 35 m respectively. Results of only the latter are presented in Fig. 7 to avoid redundancy.

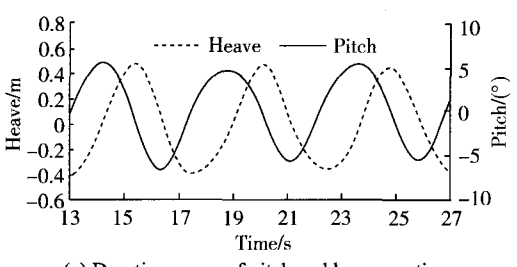

(a) Duration curve of pitch and heave motion

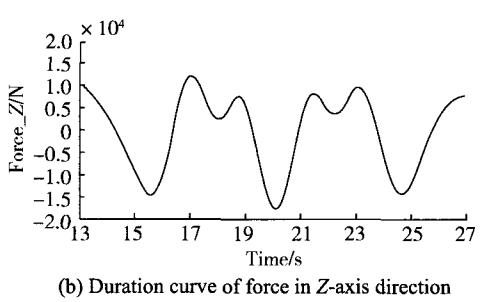

(b) Duration curve of force in *Z*-axis direction

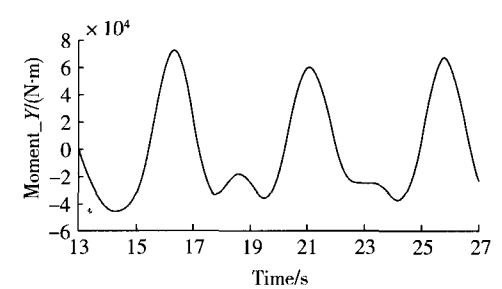

(c) Duration curve of moment on *Y*-axis

Fig. 7 Coupled motion of pitch & heave and loads under condition 3

Table 3 Comparison of results under condition 2 and condition 3

Parameter	λ=14 m	λ=35 m
Pitch/(°)	7.9	5.3
Heave/m	0.3	0.45
Force in *Z*-axis direction/kN	15.5	12.3
Moment on *Y*-axis/(MN·m)	0.149	0.064

It can be seen that there are so-called secondary wave crests in both curves of the force in *Z*-axis direction and moment on *Y*-axis, and those of force are more evident.

Table 3 is listed to represent the comparison of results under conditions with different wave length, showing that amplitude of heave increases while all the rest decrease. The values of the parameters are attained by averaging peaks of those curves.

5.4 Roll motion

As before, discussions are made according to two categories. It's worth mentioning that parameters investigated now are roll motion and moment on *X*-axis.

5.4.1 Conditions with different wave height

Results are shown below in Fig. 8. When wave height increases from 0.5 m to 1 m, amplitude of roll motion also becomes larger from 5° to 9.5°.

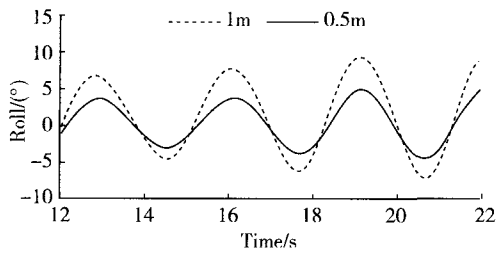

(a) Duration curve of roll motion

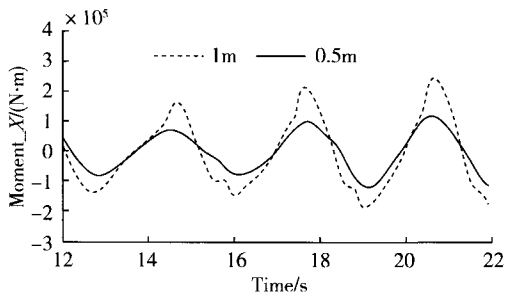

(b) Duration curve of moment on *X*-axis

Fig. 8 Roll motion and loads duration curves under conditions with different wave height

5.4.2 Conditions with different wave length

Results of condition 3 are presented in Fig. 9. Wave crests of the duration curve of roll motion become rather flat, and secondary wave crests of the duration curve of moment are quite evident.

Table 4 is listed below to show the comparison of results under conditions with different wave length, saying that both of the amplitudes decrease and that amplitude of roll motion drops by nearly 50%, which illustrates that wave length has great influence on roll motion. In other words, if the wave length of incident wave is similar to the platform's characteristic length, platform will roll violently.

Table 4 Comparison of results under condition 2 and condition 3

Parameter	λ=14 m	λ=35 m
Roll/(°)	10	5.4
Moment on *X*-axis/(MN·m)	0.18	0.14

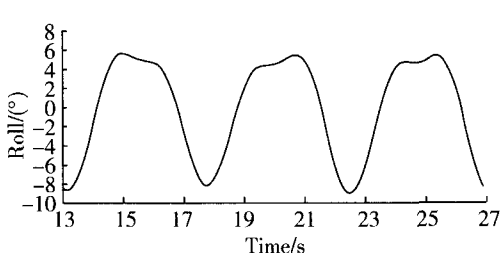

(a) Duration curve of roll motion

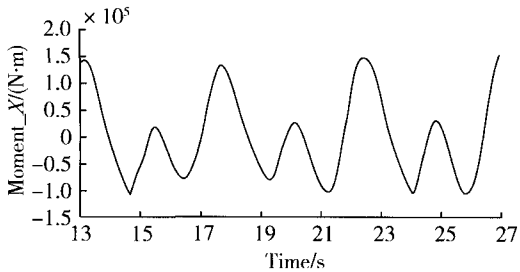

(b) Duration curve of moment on *X*-axis

Fig. 9 Roll motion and moment under condition 3

5.5 Results of condition 4

5.5.1 Coupled motion of pitch & heave

Results are shown in Fig. 10. Since duration curve of pitch motion has been shown in Fig. 5 in section 5.2, it's not presented here to avoid redundancy.

It can be seen from Fig. 5 in section 5.2 and Fig. 10 that platform moves so drastically, that amplitudes of pitch and heave motion can reach up to 10° and 1 m separately. Moreover, force and moment also increase dramatically. A set of pictures shown in Fig. 11 visually represents pitch and heave motion in one wave period.

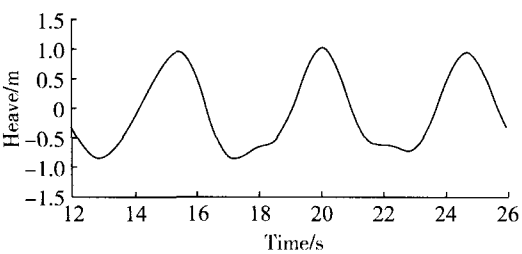

(a) Duration curve of heave motion

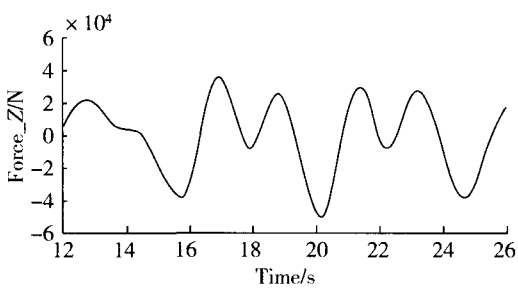

(b) Duration curve of force in *Z*-axis direction

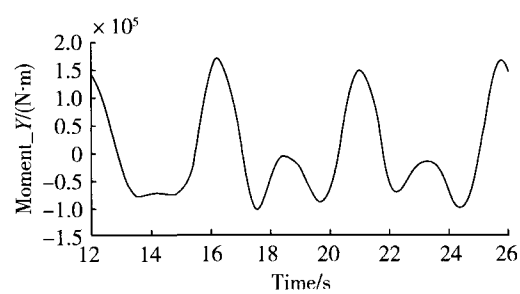

(c) Duration curve of moment on *Y*-axis

Fig. 10 Coupled motion of pitch & heave and loads under condition 4

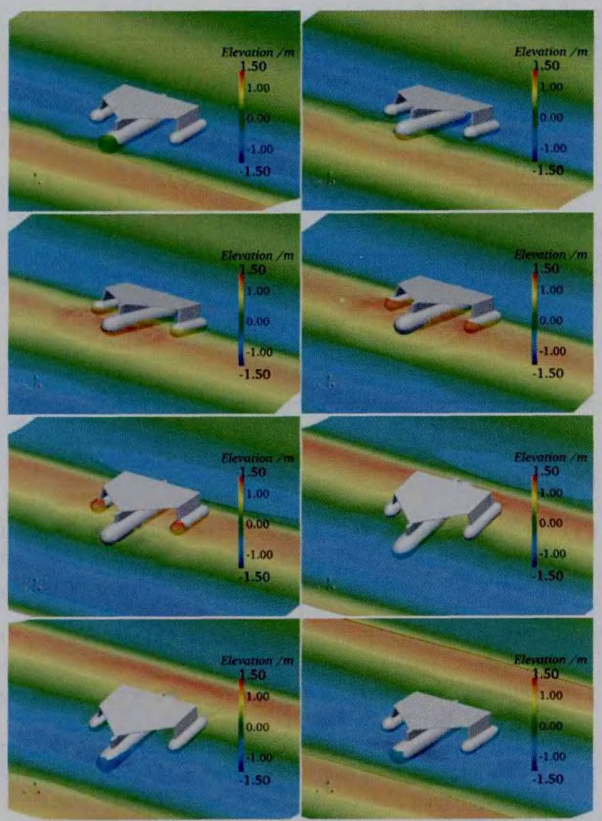

Fig. 11 Coupled motion of pitch & heave and variation of free surface elevation in one period under condition 4

Colors in Fig. 11 stand for free surface elevation. Red means higher elevation, while blue represents lower. The trim phenomenon and the influence platform exerts on wave, which causes free surface to elevate almost 1.5 m, can be clearly seen from the pictures.

5.5.2 Roll motion

Results are shown in Fig. 12. It can be seen from Fig. 12 that the maximum roll motion has exceeded 20°, and moment is several times larger than that under condition 3. A set of pictures shown in Fig. 13 vividly represents the roll motion in one wave period.

Fig. 13 shows several phenomena such as water splash and slamming, indicating the platform rolls really violently and can partly explain why the duration curve of moment changes so heavily.

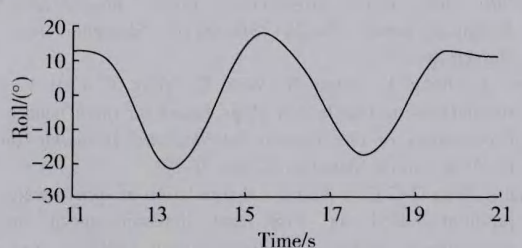

(a) Duration curve of roll motion

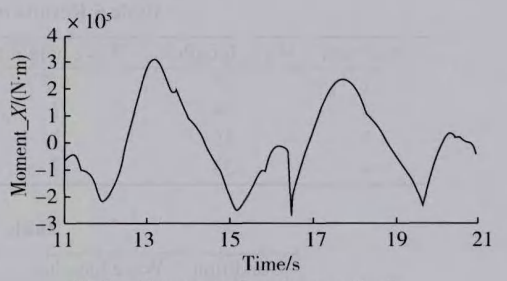

(b) Duration curve of moment on *X*-axis

Fig. 12 Roll motion and moment under condition 4

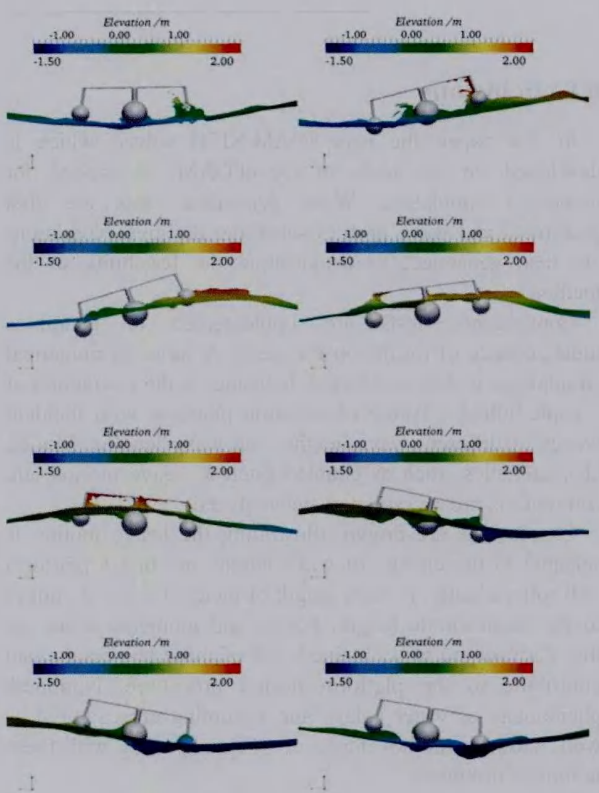

Fig. 13 Roll motion of platform and variation of free surface elevation in one period under condition 4

5.6 Summary of results

To make a better comparison and comprehension, results under all the four conditions are listed here in Table 5 and Table 6.

From those tables, we can see the motion patterns of the platform under different working conditions. Motion response as well as forces and moments of the platform are related to the wave length and wave height, but different types of motion are affected more by certain parameters of wave than others. While pitch and heave motions are more sensible to height than length of the incident wave, roll motion is strongly affected by both.

Table 5 Results of coupled motion of pitch & heave

Condition	Wave length/m	Wave height/m	Pitch/(°)	Heave/m	Force_Z/kN	Moment_Y/(MN·m)
1	14	0.5	3.5	0.08	5.7	0.066
2	14	1	7.9	0.3	15.5	0.149
3	35	1	5.3	0.45	12.3	0.064
4	35	2	11.6	1	30	0.17

Table 6 Results of roll motion

Condition	Wave length/m	Wave height/m	Roll/(°)	Moment_X/(MN·m)
1	14	0.5	5	0.11
2	14	1	9.5	0.21
3	35	1	5.4	0.14
4	35	2	14.6	0.27

6 Conclusions

In this paper, the naoe-FOAM-SJTU solver, which is developed on the tools of OpenFOAM, is applied for numerical simulation. Wave generation tests are first performed and wave profiles satisfying the given conditions are then generated, to demonstrate the feasibility of the method.

Convergence tests are implemented to guarantee independence of results on the mesh. A series of numerical simulations is then conducted, focusing on the interaction of a triple-hulled offshore observation platform with incident waves of different wave heights and wave lengths. Motion characteristics, such as coupled pitch & heave motion and roll motion, are investigated and analyzed.

Conclusions are drawn, illustrating the heave motion is sensible to the change of wave height and that a platform will roll violently, if wave length of incident wave is similar to its characteristic length. Forces and moments acting on the platform are also obtained. All of these test results can contribute to the platform design procedure. Nonlinear phenomena of water splash and slamming are captured as well, showing the advantage of CFD in dealing with these nonlinear problems.

Further research can be conducted to simulate the motion of platforms under harsher environmental conditions, such as oblique waves and extreme waves. Comparisons can be made between platforms of different shapes and parameters to provide additional feedback to designers and to help improve the ability to resist winds, waves and currents at sea.

Acknowledgement

This work is supported by the National Natural Science Foundation of China (Grant No. 50739004 and 11072154), Foundation of State Key Laboratory of Ocean Engineering of China (GKZD 010059), and the Program for Professor of Special Appointment (Eastern Scholar) at Shanghai Institutions of Higher Learning (2008007), to which the authors are most grateful.

References

Cao H, Liu Y, Wan D, Yang C (2011). Numerical simulation of solitary wave impact on fixed offshore platform. *The 7th International Workshop on Ship Hydrodynamics*, Shanghai, China, 138-143.

Cao H, Wan D (2010). Application of OpenFOAM to simulate 3-D flow past single and two tandem circular cylinder. *The Twentieth International Offshore and Polar Engineering Conference*, Beijing, China, 702-709.

Carrica PM, Fu H, Stern F (2011). Computations of self-propulsion free to sink and trim and of motions in head waves of the KRISO container ship (KCS) model. *Applied Ocean Research*, **33**(4), 309-320.

Carrica PM, Wilson RV, Noack RW, Stern F (2007). Ship motions using single-phase level set with dynamic overset grids. *Computers & Fluids*, **36**(9), 1415-1433.

Cha J, Wan D (2011). Numerical wave generation and absorption based on OpenFOAM. *The Ocean Engineering*, **29**(3), 1-12.

Chen J, Zhu D (2010). Numerical simulations of wave-induced ship motions in time domain by a Rankine panel method. *Journal of Hydrodynamics, Ser. B*, **22**(3), 373-380.

Chen X (2011). Motions simulation of a tank moving in regular wave. *Ship Science and Technology*, **33**(2), 24-27.

He W, Zhou Z, Cheng J (1998). Numerical algorithm for predicting large amplitude motion of ship in head waves. *Shipbuilding of China* (1), 42-51.

Issa R (1986). Solution of the implicitly discretised fluid flow equations by operator-splitting. *Journal of Computational Physics*, **62**(1), 40-65.

Rusche H (2002). *Computational fluid dynamics of dispersed two-phase flows at high phase fractions*. PhD thesis, Imperial College of London, London, 343.

Shen Z, Cao H, Ye H, Wan D (2012). *The manual of CFD solver for ship and ocean engineering flows: naoe-FOAM-SJTU*. Technical report, No.2012SR118110, Shanghai Jiao Tong University.

Shen Z, Jiang L, Miao S, Wan D, Yang C (2011). RANS simulations of benchmark ships based on open source code. *Proceedings of the Seventh International Workshop on Ship Hydrodynamics*, Shanghai, China, 76-82.

Shen Z, Wan D (2011). Numerical simulation of sphere water entry problem based on VOF and dynamic mesh methods. *Proceedings of the 21st International Offshore and Polar Engineering Conference*, Maui, USA, 695-702.

Shen Z, Wan D (2012). RANS computations of added resistance and motions of ship in head waves. *Proceedings of the Twenty-second International Offshore and Polar Engineering Conference (ISOPE)*, Rhodes, Greece, 1096-1103.

Wilson RV, Carrica PM, Stern F (2006). Unsteady RANS method for ship motions with application to roll for a surface combatant. *Computers & Fluids*, **35**(5), 501-524.

Wu C, Zhu D, Gu M (2008). N-S CFD simulation of wave-induced ship motions in regular head waves. *Journal of Ship Mechanics*, **12**(5), 692-696.

Yang B, Shi A, Wu M (2011). Calculation of RAO of ship motions in regular head waves based on CFD. *Ship Engineering*, **33**(S2), 32-35.

Author biographies

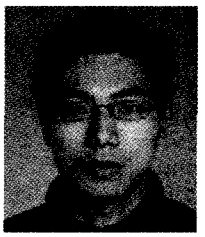

Yuanchuan Liu is a graduate student in School of Naval Architecture, Ocean and Civil Engineering, Shanghai Jiao Tong University. His current research field includes computational simulations of motion responses of platforms in waves.

Decheng Wan is a professor of school of Naval Architecture, Ocean and Civil Engineering, Shanghai Jiao Tong University, and a distinguished professor of Shanghai Eastern Scholar. His research interests include marine hydrodynamics and computational fluid dynamics, marine numerical wave tank, nonlinear wave theory, fluid-structure interaction, high performance computation on complex flows, *etc.*